TR-2015-06

DEM-PM Contact Model with Multi-Step Tangential Contact Displacement History

Jonathan Fleischmann

April 24, 2015

Abstract

We provide a brief overview of the Discrete Element Method (DEM) for modeling large frictional contact problems in granular flow dynamics and quasi-static geomechanics applications. In terms of contact, DEM can be divided into two approaches: the Constraint Method (CM) or rigid-body approach, and the Penalty Method (PM) or soft-body approach. We give a detailed presentation of a DEM-PM contact model that includes multi-time-step tangential contact displacement history. We compare results from direct shear simulations performed with Chrono using this contact model to results from identical simulations using contact models that include either no tangential contact displacement history or only single-time-step tangential contact displacement history. We show that neither of the latter two models are able to accurately model the direct shear test. In particular, the ratio of shear stress to normal stress during direct shear simulations is under-predicted by a factor of about ten when the true tangential contact displacement history model is *not* used. The new multi-step tangential contact displacement history model we have implemented in Chrono was validated using direct shear simulations of small randomly packed specimens of $1,800$ and $5,000$ identical spheres. The shear-displacement curves obtained from Chrono were compared against physical direct shear experiments performed on identical glass spheres as well as against results obtained from LIGGGHTS, an open-source DEM code that specializes in granular simulations. These comparisons show that the tangential contact displacement history model currently implemented in Chrono is (1) comparable to the model implemented in LIGGGHTS, and (2) capable of accurately reproducing results from physical tests typical of the field of geomechanics. In the appendices, we provide the details of the DEM-PM contact models currently implemented in Chrono, as well as some alternative contact models found in the literature.

Contents

1 The Discrete Element Method

Two alternative approaches have emerged as viable solutions for large frictional contact problems in granular flow dynamics and quasi-static geomechanics applications. The so-called Constraint Method (CM) or rigid-body approach is generally favored within the multibody dynamics community [1]. In this approach, individual particles in a bulk granular material are modeled as rigid bodies, and the non-penetration constraints are written as complementarity conditions which, in conjunction with a Coulomb friction law, lead to a Differential Variational Inequality (DVI) form of the Newton-Euler equations of motion [2]. Not limited by stability considerations, DVI allows for much larger time integration steps than the alternative soft-body approaches, since the latter involve large contact stiffnesses that impose strict stability conditions (CFL) on all explicit time integration algorithms. However, the DVI method involves a relatively complex and computationally costly solution sequence per time step, since it leads to a mathematical program with complementarity and equality constraints, which must be relaxed to obtain tractable linear complementarity or cone complementarity problems [3].

Widely adopted and more mature, the so-called Penalty Method (PM) or soft-body approach, generally favored within the geomechanics community [4], can be viewed either as a regularization (or smoothing) approach, which relies on a relaxation of the rigid-body assumption, or as a deformable-body approach localized to the points of contact between individual particles in a bulk granular material [5–14]. In this approach, commonly known as the Discrete Element Method (DEM), normal and tangential contact forces are calculated using various laws [15–20], which are based on the local body deformation at the point of contact. In the contact-normal direction, this local body deformation is defined as the penetration (overlap) of the two quasi-rigid bodies. In the tangential direction, the deformation is defined as the total tangential displacement incurred since the initiation of contact. Once contact forces are known, the time evolution of each body in the system is obtained by integrating the Newton-Euler equations of motion. Since in this approach the contact force-displacement law is derived from the elastic properties (the elastic or Young's modulus and Poisson's ratio) of the materials constituting the contacting bodies, the DEM-PM is capable of resolving statically indeterminate loading conditions that can exist at the particle level in random granular packings [21–23]. However, due to large contact stiffnesses and the use of explicit time integration [24], the DEM-PM approach is limited to very small time integration step-sizes to ensure stability. This leads to very long simulation times and/or the requirement of expensive hardware (e.g., distributed computing).

In the development of Chrono, we have previously favored the DVI-CM over the DEM-PM approach. The former presents a simple but evocative model of the dynamics of rigid bodies interacting through frictional contact. However, we are currently actively engaged in bringing the DEM-PM capabilities of Chrono to the same level of maturity as the DVI-CM capabilities, since we believe that both methods are necessary to accurately model granular dynamics in all possible scenarios. For example, the DVI-CM-rigid-body approach may outperform the DEM-PM-soft-body approach in the case of relatively unconstrained dynamic

granular flow; while the opposite is likely true in the case of quasi-static highly-constrained deformation of granular materials, because the latter often leads to statically indeterminate loading conditions at the particle level. Moreover, beyond modeling considerations, numerical factors also come into play. While DVI-CM methods are capable of taking large integration step-sizes Δt, the numerical solution at each time step is laborious. The point where the gains yielded by larger Δt are undermined by higher solution costs relative to DEM-PM is very problem specific, and a discussion of this falls outside the scope of this technical report.

2 The Penalty Method or Soft-Body Approach

In its most basic form, the discrete element method models a granular or particulate medium using a massive collection of distinct rigid elements having simple shapes (such as spheres). In the DEM-PM or soft-body approach, contact forces between the DEM elements is "soft", in the sense that elements are allowed to overlap before a corrective contact force is applied at the point of contact. Once such an overlap δ_n is detected, by any one of a number of contact algorithms, contact force vectors $\mathbf{F}_n$ and $\mathbf{F}_t$ normal and tangential to the contact plane at the point of contact are calculated using various constitutive laws [18,19], which are based on the local body deformation at the point of contact. In the contact-normal direction, $\mathbf{n}$, this local body deformation is defined as the penetration (overlap) of the two quasi-rigid bodies, $\boldsymbol{\delta}_n = \delta_n \mathbf{n}$. In the contact-tangential direction, the deformation is defined as the total tangential displacement incurred since the initiation of contact, which is approximated as a vector $\boldsymbol{\delta}_t$ in the contact plane.

An example of a DEM-PM contact constitutive law, a slightly modified form of which is used in the open-source codes Chrono [25] and LIGGGHTS [26], is the following viscoelastic model based on either Hookean or Hertzian contact theory:

$$\begin{aligned} \mathbf{F}_n &= f(\bar{R}\delta_n)\left(k_n \boldsymbol{\delta}_n - \gamma_n \bar{m} \mathbf{v}_n\right) \\ \mathbf{F}_t &= f(\bar{R}\delta_n)\left(-k_t \boldsymbol{\delta}_t - \gamma_t \bar{m} \mathbf{v}_t\right) , \end{aligned} \tag{1}$$

where $\boldsymbol{\delta} = \boldsymbol{\delta}_n + \boldsymbol{\delta}_t$ is the overlap or local contact displacement of two interacting bodies; $\bar{m} = m_i m_j/(m_i + m_j)$ and $\bar{R} = R_i R_j/(R_i + R_j)$ represent the effective mass and effective radius of curvature, respectively, for contacting bodies with masses m_i and m_j and contact radii of curvature R_i and R_j; and $\mathbf{v} = \mathbf{v}_n + \mathbf{v}_t$ is the relative velocity vector at the contact point. The relative velocity $\mathbf{v}$ and its normal and tangential components $\mathbf{v}_n$ and $\mathbf{v}_t$ are computed as

$$\begin{aligned} \mathbf{v} &= \mathbf{v}_j + \boldsymbol{\Omega}_j \times \mathbf{r}_j - \mathbf{v}_i - \boldsymbol{\Omega}_i \times \mathbf{r}_i \\ \mathbf{v}_n &= (\mathbf{v} \cdot \mathbf{n})\,\mathbf{n} \\ \mathbf{v}_t &= \mathbf{v} - \mathbf{v}_n , \end{aligned} \tag{2}$$

where $\mathbf{v}_i$ and $\mathbf{v}_j$ are the velocity vectors of the centers of mass of bodies i and j, $\boldsymbol{\Omega}_i$ and $\boldsymbol{\Omega}_j$ are the angular velocity vectors of bodies i and j, and $\mathbf{r}_i$ and $\mathbf{r}_j$ are the position vectors from

the centers of mass of bodies i and j to the point of contact. For Hookean contact, $f(x) = 1$ in Eq. (1); for Hertzian contact, $f(x) = \sqrt{x}$ if the coefficients k_n, k_t, γ_n, and γ_t are taken to be constant [16,17]. The normal and tangential stiffness and damping coefficients k_n, k_t, γ_n, and γ_t are obtained, through various constitutive laws derived from contact mechanics, from physically measurable quantities, such as Young's modulus, Poisson's ratio, the coefficient of restitution, etc., for the materials constituting the contacting bodies [17–20]. See the appendices for details.

The component of the overlap or contact displacement vector $\boldsymbol{\delta}$ in the contact-normal direction, $\boldsymbol{\delta}_n = \delta_n \mathbf{n}$, is obtained directly from the contact search algorithm, which provides the magnitude of the "inter-penetration" δ_n, where $\mathbf{n}$ is a unit vector normal to the contact plane. It follows that $\boldsymbol{\delta}_n$ is parallel to the normal component of the relative velocity vector $\mathbf{v}_n$ at the point of contact. However, it is important to note that the same is not true in general of the tangential component of the overlap vector, or tangential contact displacement, $\boldsymbol{\delta}_t$, and the tangential component of the relative velocity vector $\mathbf{v}_t$, both of which must lie in the contact plane, but may or may not be parallel to each other. In particular, even if there is no relative tangential velocity at the contact point, there may still be a tangential contact force needed to support static friction.

For the true tangential contact displacement history model, the vector $\boldsymbol{\delta}_t$ must be stored and updated at each time step for each contact point on a given pair of contacting bodies from the time that contact is initiated until that contact is broken. The tangential (or shear) contact displacement history vector is given by

$$\begin{aligned} \boldsymbol{\delta}_t^* &= \sum_{\Delta t} \mathbf{v}_t \Delta t \\ \boldsymbol{\delta}_t &= \boldsymbol{\delta}_t^* - (\boldsymbol{\delta}_t^* \cdot \mathbf{n})\, \mathbf{n}\,, \end{aligned} \tag{3}$$

where the first sum is taken over all time steps from the initiation of the given contact to the current time at which $\boldsymbol{\delta}_t$ is being computed. The projection of $\boldsymbol{\delta}_t^*$ onto the contact plane is necessary to ensure that $\boldsymbol{\delta}_t$ is in the contact plane at each time step.

To enforce the Coulomb friction law, if $|\mathbf{F}_t| > \mu |\mathbf{F}_n|$ at any given time step, then before the contributions of the contact forces are added to the resultant force and torque on the body, the (stored) value of $|\boldsymbol{\delta}_t|$ is scaled so that $|\mathbf{F}_t| = \mu |\mathbf{F}_n|$, where μ is the Coulomb (static and sliding) friction coefficient. For example, if $f(x) = 1$ in Eq. (1), then

$$k_t |\boldsymbol{\delta}_t| > \mu |\mathbf{F}_n| \quad \Rightarrow \quad \boldsymbol{\delta}_t \leftarrow \boldsymbol{\delta}_t \frac{\mu |\mathbf{F}_n|}{k_t |\boldsymbol{\delta}_t|}\,. \tag{4}$$

Figure 1 illustrates the DEM-PM contact model described in this section, with the normal overlap distance δ_n, the vectors $\mathbf{n}$ and $\boldsymbol{\delta}_t$, and the plane of contact (above, left and right), and with a Hookean-linear contact force-displacement law with constant Coulomb sliding friction (below, left and right).

Once the contact forces F_n and F_t are computed for each contact and their contributions are summed to obtain a resultant force and torque on each body in the system, the time

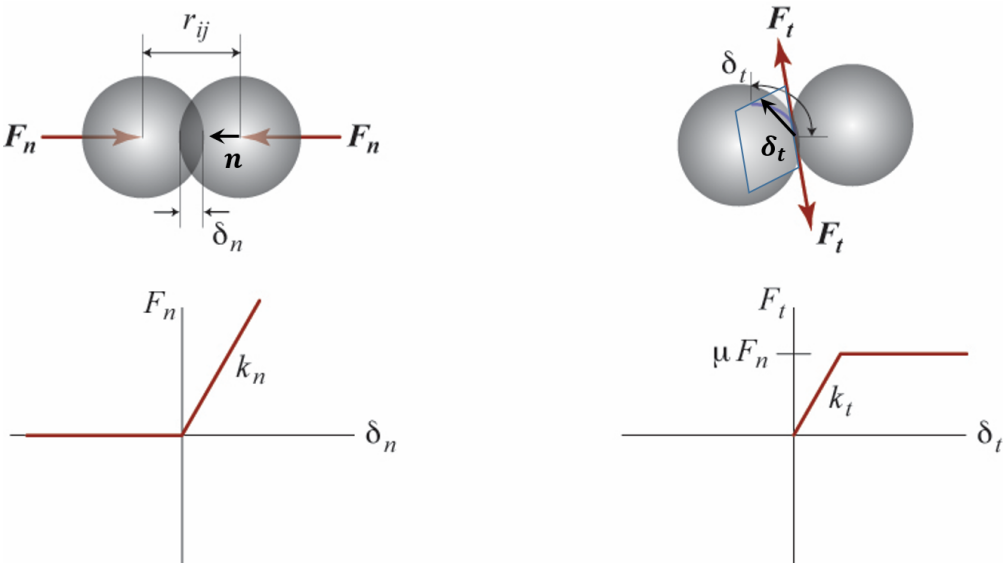

Figure 1: DEM-PM contact model described in this section, with the normal overlap distance δ_n, the vectors $\mathbf{n}$ and $\boldsymbol{\delta}_t$, and the plane of contact (above, left and right), and with a Hookean-linear contact force-displacement law with constant Coulomb sliding friction (below, left and right).

evolution of each body in the system is obtained by integrating the Newton-Euler equations of motion. However, due to large contact stiffness, DEM-PM methods are limited to very small time integration step-sizes, which lead to very long simulation times. For example, for the linear (Hookean) contact model with a central difference time integration scheme, the Courant-Friedrichs-Lewy (CFL) condition [27, 28] implies that

$$\Delta t < \Delta t_{\text{crit}} \sim \sqrt{\frac{m_{\text{min}}}{k_{\text{max}}}}\,. \tag{5}$$

Thus, as an example, if a DEM simulation using the linear (Hookean) contact model contains at least one quartz sand particle with a diameter of 0.5 mm and a mass of about $2(10^{-4})$ g, with Young's modulus $E \approx 80$ GPa and Poisson's ratio $\nu \approx 0.3$, then Eq. (6) implies that $k_n \approx 10^{12}$ N/m, which, according to Eq. (5) gives a critical (maximum stable) time integration step-size of $\Delta t_{\text{crit}} \sim 10^{-8}$ s for the system. For this reason, the stiffness of DEM particles is usually artificially softened by as much as three to four orders of magnitude to ensure a stable simulation with a more reasonable time integration step-size.

3 The Importance of Multi-Step Tangential Contact Displacement History

To test the DEM-PM contact model with tangential displacement history recently implemented in Chrono [25], we have performed direct shear simulations of small randomly packed

specimens of 1,800 and 5,000 identical spheres. For validation, we have compared the shear-displacement curves obtained from Chrono against physical direct shear experiments [29], performed on identical glass spheres of the same size and scale as in our DEM simulations. We have also compared results obtained from Chrono to results obtained from a popular open-source DEM code that specializes in granular simulations, called LIGGGHTS [26], under identical simulation conditions. These comparisons show that the tangential contact displacement history model currently implemented in Chrono is (1) comparable to the model implemented in LIGGGHTS, and (2) capable of accurately reproducing results from physical tests typical of the field of geomechanics.

Figure 2 (right) shows the (nondimensional) ratio of shear stress to normal stress for a direct shear simulation performed under constant normal stress conditions as a function of shear displacement (normalized by particle diameter). The simulation geometry in its final position is shown in Fig. 2 (left). The inside dimensions of the shear box are 6 cm in length by 6 cm in width, and the height of the granular material specimen in the box is also approximately 6 cm. The spheres have a uniform diameter of 5 mm. The random packing of 1,800 spheres was initially obtained by a "rainfall" method, after which the spheres were compacted with friction temporarily turned off to obtain a dense packing. The resulting void ratio was approximately $e = 0.4$, which corresponds to a dense packing [30,31]. For this comparison, the material properties of the spheres were taken to be those corresponding to quartz, for which the density is 2,500 kg/m^3, the inter-particle friction coefficient is $\mu = 0.5$, Poisson's ratio is $\nu = 0.3$, and the elastic modulus is $E = 8(10^{10})$ Pa, except that the elastic modulus was reduced by four orders of magnitude to $E = 8(10^6)$ Pa to ensure a stable simulation with a reasonable time integration step-size of $\Delta t = 10^{-5}$ seconds. The shear speed was 1 mm/s.

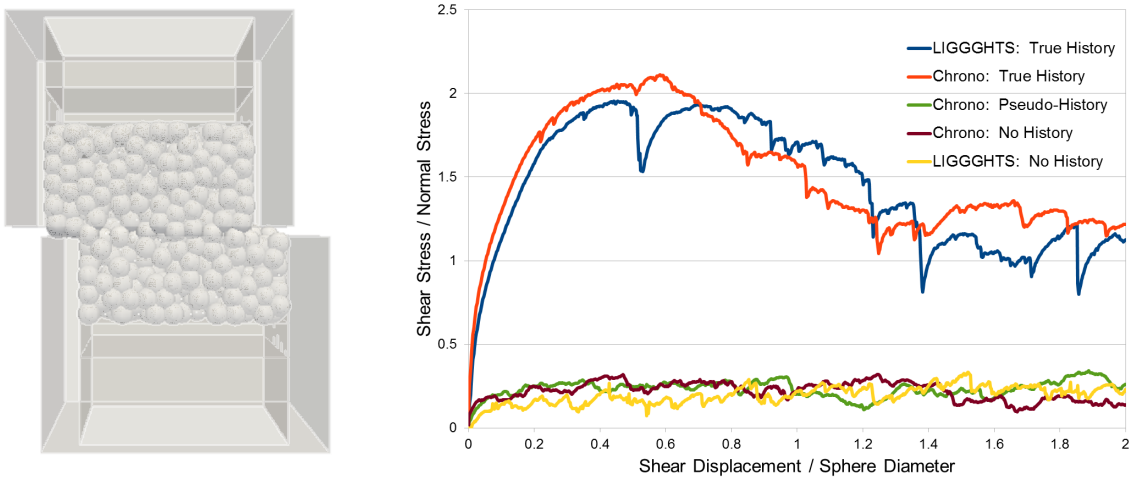

Figure 2: Direct shear simulation setup (left) and shear versus displacement results (right) obtained by Chrono [25] and LIGGGHTS [26] for 1,800 randomly packed uniform spheres using various tangential contact models.

Figure 2 (right) shows the shear-displacement curves obtained by Chrono and LIGGGHTS with the same contact model under various assumptions regarding the way tangential contact displacement history is stored and computed. The tangential contact models of "True History" and "No History" refer to whether or not tangential contact history is stored at all, and these options are also available in LIGGGHTS and other DEM codes. The tangential contact model of "Pseudo-History" is also included for comparison, since it has been argued [32] that the tangential contact displacement vector can be approximated by the product of the relative tangential velocity vector at the contact point and the time step-size at any given time. This pseudo-history approach is attractive, since it avoids the storage of a tangential contact history vector for each contact point, which must be maintained over multiple time steps for the true history approach, and for this reason the pseudo-history approximation has been adopted by some DEM codes. However, Fig. 2 shows that the pseudo-history approximation is no better than ignoring tangential displacement history altogether for the quasi-static direct shear test. This is because under quasi-static (or static) deformation conditions, the dependence of the pseudo-history approximation on the relative inter-particle tangential velocity effectively eliminates the inter-particle tangential contact force, and so renders the inter-particle friction coefficient μ effectively zero.

Also noteworthy in Fig. 2 is the fact that the inter-particle friction coefficient μ for the spheres, which could also be described as a micro-scale "inter-particle friction angle" $\phi_\mu = \tan^{-1}\mu$, is nowhere close to having the same value as the macro-scale "material friction coefficient" μ_{macro} for the bulk granular material, more commonly described as a bulk granular material friction angle $\phi = \tan^{-1}\mu_{\text{macro}}$, which is the material parameter that defines the yield surface for the bulk granular material according the Mohr-Coulomb yield criterion. The material friction angle ϕ is also known as the angle of repose for the bulk granular material. Nor should it be surprising that $\phi \neq \phi_\mu$, since, as noted in [33], even if the inter-particle friction coefficient μ (and hence the micro-scale friction angle ϕ_μ) is zero, the bulk granular material friction angle ϕ will in general not be zero. Rather, if $\mu = 0$, then $\phi = \psi$, where ψ is the dilation angle of the granular material. (Typically, $\psi \approx 15^\circ$ for densely packed well-graded sands [34].) In particular, we note from Fig. 2 that, when the tangential contact displacement history model is used, while $\mu = 0.5$ and hence $\phi_\mu \approx 26.6^\circ$ for the spheres, the peak ratio of shear stress to normal stress for the bulk granular material is $\mu_{\text{macro}} \approx 2$, and hence $\phi_p \approx 63^\circ$; and the residual ratio of shear stress to normal stress for the bulk granular material is $\mu_{\text{macro}} \approx 1$, and hence $\phi_r \approx 45^\circ$. On the other hand, when the tangential contact displacement history model is *not* used, $\mu_{\text{macro}} \approx 0.25$ throughout the simulations, and hence $\phi_p = \phi_r = \phi \approx 14^\circ$. Note that all of these results are obtained in the absence of any rolling or spinning friction.

It is also worth pointing out that for standard graded (quartz) sand (ASTM C 778-06), which has a log-normal particle size distribution with mean diameter $D_{50} = 0.35$ mm and coefficient of uniformity $C_u = 1.7$, the value of the residual bulk material friction angle obtained by the direct shear test, as well as the angle of repose, is $\phi_r \approx 30^\circ$ [35]; while the peak bulk material friction angle ϕ_p obtained by the direct shear test strongly depends on the initial packing density of the granular material. According to Bardet [30], typical

values of the peak friction angle and the residual friction angle for densely packed well-graded sands are $38^\circ < \phi_p < 46^\circ$ and $30^\circ < \phi_r < 34^\circ$, respectively. These values of the peak and residual friction angles are strongly dependent, however, on the particle size distribution [36], which is why the residual friction angle for uniform quartz spheres cannot be expected to be the same as that of quartz spheres (or well-rounded quartz sand) with a log-normal particle size distribution. In [37] we performed 3D DEM simulations of direct (ring) shear tests with periodic boundary conditions using a linear (Hookean) contact law with true tangential contact displacement history, and we showed that for ASTM C 778-06 standard graded (Ottawa) sand with a log-normal particle size distribution, with no rolling friction and with sand particles modeled as spheres (of different sizes), the correct macro-scale residual material friction angle of $\phi_r = 30^\circ$ is reproduced exactly. For the micro-scale inter-particle friction coefficient in these simulations, we used $\mu = 0.5$ (or $\phi_\mu = 26.6^\circ$), which is considered by Mitchell and Soga [31] to be "reasonable for quartz, both wet and dry."

4 Validation Against Direct Shear Experiments With Uniform Glass Beads

To verify that the DEM-PM contact model with true tangential displacement history currently implemented in Chrono does indeed accurately model the micro-scale physics and emergent macro-scale properties of a simple granular material, Fig. 3 shows shear versus displacement curves obtained from both experimental [29] (left) and simulated (right) direct shear tests, performed under constant normal stresses of 3.1, 6.4, 12.5, and 24.2 kPa, on $5,000$ uniform glass beads. The simulation geometry in its final position is similar to that shown in Fig. 2 (left), except that the inside dimensions of the shear box are now 12 cm in length by 12 cm in width, and the height of the granular material specimen in the box is still approximately 6 cm. In both the experimental and simulated direct shear tests, the glass spheres have a uniform diameter of 6 mm, and the random packing of $5,000$ spheres was initially obtained by a "rainfall" method, after which the spheres were compacted by the confining normal stress without adjusting the inter-particle friction coefficient. The DEM simulations were performed in Chrono using a Hertzian normal contact force model and true tangential contact displacement history with Coulomb friction. The material properties of the spheres in the simulations were taken to be those corresponding to glass [29], for which the density is $2,550$ kg/m^3, the inter-particle friction coefficient is $\mu = 0.18$, Poisson's ratio is $\nu = 0.22$, and the elastic modulus is $E = 4(10^{10})$ Pa, except that the elastic modulus was again reduced by four orders of magnitude to $E = 4(10^6)$ Pa to ensure a stable simulation with a reasonable time integration step-size of $\Delta t = 10^{-5}$ seconds. The shear speed was 1 mm/s.

Figure 3 shows that the DEM-PM direct shear simulations performed in Chrono on $5,000$ glass spheres does a fairly good job of matching the physical experiments for all but the highest normal stress of 24.2 kPa. This observed error in the simulation results, which increases with increasing normal stress, is consistent with the fact that the stiffness; i.e., the

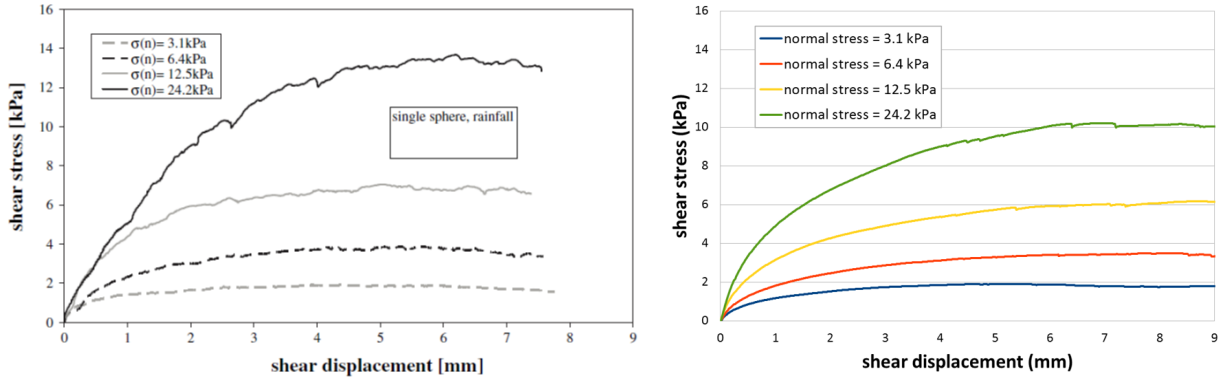

Figure 3: Direct shear test results for $5,000$ randomly packed uniform glass beads obtained by experiment [29] (left) and DEM simulations using Chrono (right), under constant normal stresses of 3.1, 6.4, 12.5, and 24.2 kPa. For the DEM simulations, an elastic modulus of $E = 4(10^6)$ Pa is used, which is $10,000$ times softer than the true elastic modulus of the glass beads used in the experiment.

elastic modulus, used for the spheres in the DEM simulations is four orders of magnitude smaller than the stiffness of true glass beads. To explore the effect that the value of the elastic modulus has on the DEM direct shear results, we have also performed DEM simulations using an elastic modulus of $E = 4(10^7)$ Pa for the spheres, which is still three orders of magnitude smaller than the true elastic modulus of glass beads. Figure 4 shows shear versus displacement curves obtained from both experimental [29] (left) and simulated (right) direct shear tests, performed under constant normal stresses of 3.1, 6.4, 12.5, and 24.2 kPa, on $5,000$ uniform glass beads. All parameters for the DEM simulations of Fig. 4 are identical to those reported for Fig. 3, except that the elastic modulus for the spheres is $E = 4(10^7)$ Pa rather than $E = 4(10^6)$ Pa.

Figure 4 shows that increasing the value of the elastic modulus of the spheres in the DEM direct shear simulations by an order of magnitude; i.e., using a contact stiffness for the DEM spheres that is three rather than four orders of magnitude smaller than the physically correct contact stiffness, results in a peak and residual shear stress that is much closer to the experimentally observed values for all four of the constant normal stresses tested. This is a significant observation, since it has often been argued in the DEM literature that decreasing the value of the elastic modulus to allow a larger stable time step-size should only affect the *elastic* portion of the shear displacement curve for the bulk granular material. A comparison of Figs. 3 and 4, however, while confirming this difference in the elastic portion of the shear-displacement curve, also reveals a significant difference in the *plastic* or post-yield portion of the shear-displacement curve for the direct shear test, in particular the peak and residual shear stresses, and the corresponding peak and residual friction angles, for all four of the constant normal stresses tested.

A final note is in order regarding the packing densities or void ratios of the physical experiments and DEM simulations used to obtain the direct shear results reported in this

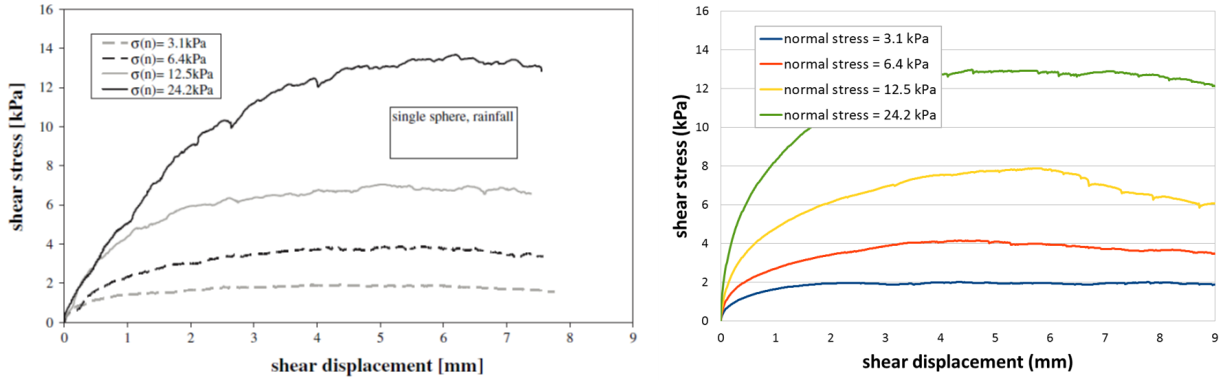

Figure 4: Direct shear test results for $5,000$ randomly packed uniform glass beads obtained by experiment [29] (left) and DEM simulations using Chrono (right), under constant normal stresses of 3.1, 6.4, 12.5, and 24.2 kPa. For the DEM simulations, an elastic modulus of $E = 4(10^7)$ Pa is used, which is $1,000$ times softer than the true elastic modulus of the glass beads used in the experiment.

section. For the direct shear experiments on uniform glass beads performed by [20], the void ratio was reported as $e \approx 0.7$, which corresponds to a loose packing [30, 31]. However, if we compute the void ratio $e = \mathrm{V}_{\text{void}}/\mathrm{V}_{\text{solid}}$ for the granular material specimens in the DEM simulations, by computing the volume of the solids as $\mathrm{V}_{\text{solid}} = 5,000(4/3)\pi(0.003)^3$ m^3 and the volume of the voids as $\mathrm{V}_{\text{void}} = \mathrm{V}_{\text{total}} - \mathrm{V}_{\text{solid}}$, then for the DEM simulations with an elastic modulus of $E = 4(10^6)$ Pa (which is $10,000$ softer than the physically correct value), although an identical rainfall method was used as in the physical experiments to obtain a loose packing, the application of the normal stresses results in an overlap of the DEM spheres that is so significant that the void ratio e as calculated above is no longer representative of the packing geometry. Thus, we observe that for the DEM simulations with an elastic modulus of $E = 4(10^6)$ Pa, the void ratios were calculated as $e = 0.58$, 0.54, 0.48, and 0.40 for the normal stresses of 3.1, 6.4, 12.5, and 24.2 kPa, respectively; while for the DEM simulations with an elastic modulus of $E = 4(10^7)$ Pa, the void ratios were calculated as $e = 0.66$, 0.65, 0.62, and 0.60, respectively, for the same normal stresses.

A DEM-PM Contact Models Currently Implemented in Chrono

The specific Hookean and Hertzian contact models currently implemented in Chrono [25] follow those of LIGGGHTS [26]. For both models, we let $f(x) = 1$ in Eq. (1), and we let k_n and k_t depend on δ_n and $\bar{R}$ directly for the Hertzian model rather than letting $f(x) = \sqrt{x}$ in Eq. (1) as in [16]. For Hookean contact:

$$\begin{aligned} k_n &= \frac{16}{15}\bar{E}\sqrt{\bar{R}}\left(\frac{15\bar{m}V^2}{16\bar{E}\sqrt{\bar{R}}}\right)^{1/5} & \gamma_n &= \sqrt{\frac{4\bar{m}k_n}{1+\left(\frac{\pi}{\ln(\mathrm{COR})}\right)^2}} \geq 0 \\ k_t &= k_n & \gamma_t &= \gamma_n\,, \end{aligned} \tag{6}$$

and for Hertzian contact:

$$\begin{aligned} k_n &= \frac{4}{3}\bar{E}\sqrt{\bar{R}\delta_n} & \gamma_n &= -2\sqrt{\frac{5}{6}}\beta\sqrt{\frac{3}{2}\bar{m}k_n} \geq 0 \\ k_t &= 8\bar{G}\sqrt{\bar{R}\delta_n} & \gamma_t &= -2\sqrt{\frac{5}{6}}\beta\sqrt{\bar{m}k_t} \geq 0\,, \end{aligned} \tag{7}$$

where $\bar{E}$ and $\bar{G}$, are effective elastic (Young's) and shear moduli, respectively, for the materials in contact, COR is the coefficient of restitution for the contacting pair, V is a characteristic impact velocity (needed for the Hookean model), and

$$\beta = \frac{\ln(\mathrm{COR})}{\sqrt{\ln^2(\mathrm{COR}) + \pi^2}}\,. \tag{8}$$

Equation (8) follows the model of [38]. According to [7], if E_i and E_j are the elastic moduli for the two bodies in contact, then the effective elastic and shear moduli are given by

$$\begin{aligned} \bar{E} &= \left(\frac{1-\nu_i^2}{E_i} + \frac{1-\nu_j^2}{E_j}\right)^{-1} \\ \bar{G} &= \left(\frac{2(2+\nu_i)(1-\nu_i)}{E_i} + \frac{2(2+\nu_j)(1-\nu_j)}{E_j}\right)^{-1}\,, \end{aligned} \tag{9}$$

where ν_i and ν_j are Poisson's ratios for the two materials in contact. As stated earlier, the effective contact radius of curvature and mass are given by

$$\bar{R} = \left(\frac{1}{R_i} + \frac{1}{R_j}\right)^{-1} \qquad \bar{m} = \left(\frac{1}{m_i} + \frac{1}{m_j}\right)^{-1}\,, \tag{10}$$

for contacting bodies with masses m_i and m_j and radii of curvature R_i and R_j at the point of contact.

B Alternative DEM-PM Contact Models

Another contact model that could be employed is the modified Hertzian-Mindlin model adopted in the popular commercial DEM codes PFC^{2D} and PFC^{3D}, for which, according to [39], the stiffness coefficients k_n and k_t in Eq. (1) with $f(x) = 1$ are given by

$$\begin{aligned} k_n &= \left(\frac{4\bar{G}}{3(1-\bar{\nu})}\right)\sqrt{\bar{R}\delta_n} \\ k_t &= \left(\frac{2(\bar{G}^2 6(1-\bar{\nu})\bar{R})^{1/3}}{2-\bar{\nu}}\right) F_n \,. \end{aligned} \tag{11}$$

Alternatively, in the (Hertzian) contact model adopted by [17], the stiffness coefficients k_n and k_t are given by

$$\begin{aligned} k_n &= \frac{4\bar{G}}{3(1-\bar{\nu})} \\ k_t &= \frac{4\bar{G}}{2-\bar{\nu}} \,, \end{aligned} \tag{12}$$

with $f(x) = \sqrt{x}$ in Eq. (1). Note that the normal stiffness coefficient k_n given in Eq. (12) together with $f(x) = \sqrt{x}$ in Eq. (1) results in the same normal stiffness as the coefficient k_n given in Eq. (11) with $f(x) = 1$ in Eq. (1).

Alternative contact models for either linear or nonlinear (Hookean or Hertzian) normal and tangential contact force-displacement laws can be derived directly from Hertz-Mindlin contact theory [40, 41]. According to Deresiewicz [41], if two identical spheres of radius R are compressed statically by a force F_n directed along their line of centers, then the spheres are in contact on a planar circular area of radius R_c, with

$$R_c = \left(\frac{3(1-\nu^2)}{4E} R F_n\right)^{1/3} \,, \tag{13}$$

where E and ν are the elastic Young's modulus and Poisson's ratio for the material constituting the spheres. According to Deresiewicz, the initial normal and tangential contact stiffnesses between the spheres are then given by

$$\begin{aligned} k_n &= \left(\frac{2G}{1-\nu}\right) R_c \\ k_t &= \left(\frac{4G}{2-\nu}\right) R_c \,, \end{aligned} \tag{14}$$

where G is the elastic shear modulus of the sphere material. The normal and tangential contact forces F_n and F_t are then given by Eq. (1) with $f(x) = 1$.

Note that the Hertz-Mindlin contact model described in Eqs. (13) and (14) is nonlinear, because the normal and tangential inter-particle contact stiffnesses k_n and k_t given in Eq. (14) depend on the normal contact force F_n via Eq. (13). However, for certain applications where

a granular material may be confined by a relatively constant hydrostatic pressure, one may assume that the contact stiffnesses k_n and k_t are roughly constant within a small range of deformation about an initial nonzero isotropic compressive stress σ_0. In the case of a dense packing, this initial isotropic compressive stress σ_0 produces an initial normal contact force $F_n = F_0 \approx \sqrt{2}R^2\sigma_0$; in the case of a loose packing, $F_n = F_0 \approx 4R^2\sigma_0$ [21]. From Eq. (13) with $F_n = F_0$, this initial normal contact force produces an initial contact radius R_0, which can then be used to linearize the contact force-displacement laws by providing constant values for k_n and k_t via Eq. (14) with $R_c = R_0$.

It will be noted that a significant degree of variation exists in the literature for the exact values of the contact stiffness coefficients k_n and k_t. The same is true for the mass proportional damping coefficients γ_n and γ_t. In fact, the latter are frequently simply chosen sufficiently large to eliminate numerical noise in the DEM simulations. This was done, for example, in the direct shear simulations performed by us in [37], where the damping coefficients in Eq. (1) were taken to be $\gamma_n = 40$ s^{-1} and $\gamma_t = 20$ s^{-1}. Moreover, while we have shown that it is indeed necessary to use contact stiffnesses k_n and k_t that are large *enough* (in terms of order of magnitude) to obtain accurate shear-displacement curves from direct shear DEM simulations, the precise values of k_n and k_t seem less important. Again, for the direct shear simulations performed in [37] on well-graded quartz sand, modeled as spheres with a log-normal particle size distribution, constant values of $k_n = 10^9$ N/mm and $k_t = 8(10^8)$ N/mm were used, where the normal stiffness k_n was chosen to be on the order of magnitude corresponding to the normal stiffness predicted by nonlinear Hertz-Mindlin theory for quartz spheres of diameter $D \approx 0.5$ mm if a radial strain of $\epsilon_r = 0.001$ at the point of contact is assumed, where the modulus of elasticity for quartz is $E = 8(10^{10})$ Pa; and the tangential stiffness was obtained from the ratio $k_t/k_n = 2\,(1-\nu)\,/(2-\nu)$ [15], which can be obtained from Eq. (14), where Poisson's ratio for quartz is $\nu = 0.3$. Despite these simplifications, the bulk granular material friction angle $\phi = 30^\circ$ obtained from the DEM-PM direct shear simulations in [37] matched that of the physical modeled sand *exactly*. The only other material parameter that needed to be specified, in addition to the particle size distribution, was the inter-particle friction coefficient $\mu = 0.5$ for quartz-on-quartz. This relative insensitivity of the quasi-static direct shear behavior of a bulk granular material to the details of the inter-particle contact model, and in particular the exact values of the coefficients k_n, k_t, γ_n, and γ_t (except for order of magnitude), is in striking contrast, however, to the sensitivity of the direct shear behavior of the granular material to whether or not the inter-particle contact model employed uses multi-step tangential contact displacement history, which was used in [37].

References

[1] A. Tasora and M. Anitescu. A convex complementarity approach for simulating large granular flows. *Journal of Computational and Nonlinear Dynamics*, 5(3):1–10, 2010.

[2] D. E. Stewart. Rigid-body dynamics with friction and impact. *SIAM Review*, 42(1):3–39, 2000.

[3] M. Anitescu and A. Tasora. An iterative approach for cone complementarity problems for nonsmooth dynamics. *Computational Optimization and Applications*, 47(2):207–235, 2010.

[4] C. O'Sullivan. Particle-based discrete element modeling: Geomechanics perspective. *Int. J. Geomech.*, 11(6):449–464, 2011.

[5] P. Cundall. A computer model for simulating progressive large-scale movements in block rock mechanics. In *Proceedings of the International Symposium on Rock Mechanics. Nancy, France*, 1971.

[6] P. Cundall and O. Strack. A discrete element model for granular assemblies. *Geotechnique*, 29:47–65, 1979.

[7] K. L. Johnson. *Contact mechanics*. Cambridge University Press, 1987.

[8] P. A. Cundall. Formulation of a three-dimensional distinct element model–Part I. A scheme to detect and represent contacts in a system composed of many polyhedral blocks. *International Journal of Rock Mechanics and Mining Sciences & Geomechanics Abstracts*, 25(3):107–116, 1988.

[9] H. M. Jaeger, S. R. Nagel, and R. P. Behringer. Granular solids, liquids, and gases. *Rev. Mod. Phys.*, 68:1259–1273, Oct 1996.

[10] N. V. Brilliantov, F. Spahn, J.-M. Hertzsch, and T. Pöschel. Model for collisions in granular gases. *Physical Review E*, 53(5):5382, 1996.

[11] L. Vu-Quoc and X. Zhang. An elastoplastic contact force–displacement model in the normal direction: displacement–driven version. *Proceedings of the Royal Society of London. Series A: Mathematical, Physical and Engineering Sciences*, 455(1991):4013–4044, 1999.

[12] L. Vu-Quoc, L. Lesburg, and X. Zhang. An accurate tangential force–displacement model for granular-flow simulations: Contacting spheres with plastic deformation, force-driven formulation. *Journal of Computational Physics*, 196(1):298–326, 2004.

[13] S. Luding. *Molecular Dynamics Simulations of Granular Materials*, pages 297–324. Wiley-VCH Verlag GmbH, 2005.

[14] T. Pöschel and T. Schwager. *Computational granular dynamics: models and algorithms*. Springer, 2005.

[15] D. Elata and J. G. Berryman. Contact force-displacement laws and the mechanical behavior of random packs of identical spheres. *Mechanics of Materials*, 24:229–240, 1996.

[16] L. E. Silbert, D. Ertaş, G. S. Grest, T. C. Halsey, D. Levine, and S. J. Plimpton. Granular flow down an inclined plane: Bagnold scaling and rheology. *Physical Review E*, 64(5):051302, 2001.

[17] H. P. Zhang and H. A. Makse. Jamming transition in emulsions and granular materials. *Physical Review E*, 72(1):011301, 2005.

[18] H. Kruggel-Emden, E. Simsek, S. Rickelt, S. Wirtz, and V. Scherer. Review and extension of normal force models for the discrete element method. *Powder Technology*, 171:157–173, 2007.

[19] H. Kruggel-Emden, S. Wirtz, and V. Scherer. A study of tangential force laws applicable to the discrete element method (DEM) for materials with viscoelastic or plastic behavior. *Chem. Eng. Sci.*, 63:1523–1541, 2008.

[20] G. Hu, Z. Hu, B. Jian, L. Liu, and H. Wan. On the determination of the damping coefficient of non-linear spring-dashpot system to model Hertz contact for simulation by discrete element method. *Journal of Computers*, 6(5):984–988, 2011.

[21] J. A. Fleischmann, W. J. Drugan, and M. E. Plesha. Direct micromechanics derivation and DEM confirmation of the elastic moduli of isotropic particulate materials, Part I: No particle rotation. *J. Mech. Phys. Solids*, 61(7):1569–1584, 2013.

[22] J. A. Fleischmann, W. J. Drugan, and M. E. Plesha. Direct micromechanics derivation and DEM confirmation of the elastic moduli of isotropic particulate materials, Part II: Particle rotation. *J. Mech. Phys. Solids*, 61(7):1585–1599, 2013.

[23] N. P. Kruyt. Micromechanical study of elastic moduli of three-dimensional granular assemblies. *Int. J. Solids Struct.*, 51:2336–2344, 2014.

[24] K. Samiei, B. Peters, M. Bolten, and A. Frommer. Assessment of the potentials of implicit integration method in discrete element modelling of granular matter. *Computers & Chemical Engineering*, 49:183–193, 2013.

[25] Chrono Website. `http://projectchrono.org/chronoengine/`. Accessed: 2015-03-19.

[26] LIGGGHTS Website. `http://www.cfdem.com/`. Accessed: 2015-03-19.

[27] R. D. Cook, D. S. Malkus, M. E. Plesha, and R. J. Witt. *Concepts and Applications of Finite Element Analysis*. John Wiley and Sons, 2002.

[28] C. O'Sullivan and J. D. Bray. Selecting a suitable time step for discrete element simulations that use the central difference time integration scheme. *Engineering Computations*, 21(2-4):278–303, 2004.

[29] J. Härtl and J. Y. Ooi. Experiments and simulations of direct shear tests: porosity, contact friction and bulk friction. *Granular Matter*, 10(4):263–271, 2008.

[30] J.-P. Bardet. *Experimental Soil Mechanics*. Prentice Hall, 1997.

[31] J. K. Mitchell and K. Soga. *Fundamentals of Soil Behavior*. John Wiley and Sons, 2005.

[32] T. Heyn. *On the Modeling, Simulation, and Visualization of Many-Body Dynamics Problems with Friction and Contact*. PhD thesis, Department of Mechanical Engineering, University of Wisconsin–Madison, `http://sbel.wisc.edu/documents/TobyHeynThesis\_PhDfinal.pdf`, 2013.

[33] J. A. Fleischmann. *Micromechanics-Based Continuum Constitutive Modeling of Isotropic Non-Cohesive Particulate Materials, Informed and Validated by the Discrete Element Method*. PhD thesis, Department of Engineering Mechanics, University of Wisconsin–Madison, 2013.

[34] P. A. Vermeer and R. de Borst. Non-associated plasticity for soils, concrete and rock. *Heron*, 29(3):1–64, 1984.

[35] G.-C. Cho, J. Dodds, and J. C. Santamarina. Particle shape effects on packing density, stiffness, and strength: Natural and crushed sands. *J. Geotech. Geoenviron. Eng.*, 132(5):591–602, 2006.

[36] Y. P. Cheng and N. H. Minh. DEM investigation of particle size distribution effect on direct shear behaviour of granular agglomerates. In *Powders and Grains 2009, Proceedings of the 6th International Conference on Micromechanics of Granular Media*, pages 401–404, 2009.

[37] J. A. Fleischmann, M. E. Plesha, and W. J. Drugan. Quantitative comparison of two-dimensional and three-dimensional discrete element simulations of nominally two-dimensional shear flow. *Int. J. Geomech.*, 13(3):205–212, 2013.

[38] K. H. Hunt and F. R. E. Crossley. Coefficient of restitution interpreted as damping in vibroimpact. *J. Appl. Mech.*, 42(2):440–445, 1975.

[39] L. Jing and O. Stephansson. *Fundamentals of Discrete Element Methods for Rock Engineering: Theory and Applications*. Elsevier B.V., 2007.

[40] J. Duffy and R. D. Mindlin. Stress-strain relations and vibrations of a granular medium. *J. Appl. Mech.*, 24:585–593, 1957.

[41] H. Deresiewicz. Mechanics of granular matter. In H. L. Dryden and Th. von Kármán, editors, *Advances in Applied Mechanics*, volume 5, pages 233–306. Academic Press Inc., New York, 1958.